Neurosci. Bull. August, 2019, 35(4):709–723
https://doi.org/10.1007/s12264-019-00385-6

www.neurosci.cn
www.springer.com/12264

ORIGINAL ARTICLE

Cortical Organization of Centrifugal Afferents to the Olfactory Bulb: Mono- and Trans-synaptic Tracing with Recombinant Neurotropic Viral Tracers

Pengjie Wen[1,2] · Xiaoping Rao[1] · Liuying Xu[3] · Zhijian Zhang[1] · Fan Jia[1] · Xiaobin He[1] · Fuqiang Xu[1,4]

Received: 24 July 2018 / Accepted: 14 September 2018 / Published online: 8 May 2019
© Shanghai Institutes for Biological Sciences, CAS 2019

Abstract Sensory processing is strongly modulated by different brain and behavioral states, and this is based on the top–down modulation. In the olfactory system, local neural circuits in the olfactory bulb (OB) are innervated by centrifugal afferents in order to regulate the processing of olfactory information in the OB under different behavioral states. The purpose of the present study was to explore the organization of neural networks in olfactory-related cortices and modulatory nuclei that give rise to direct and indirect innervations to the glomerular layer (GL) of the OB at the whole-brain scale. Injection of different recombinant attenuated neurotropic viruses into the GL showed that it received direct inputs from each layer in the OB, centrifugal inputs from the ipsilateralanterior olfactory nucleus (AON), anterior piriform cortex (Pir), and horizontal limb of diagonal band of Broca (HDB), and various indirect inputs from bilateral cortical neurons in the AON, Pir, amygdala, entorhinal cortex, hippocampus, HDB, dorsal raphe, median raphe and locus coeruleus. These results provide a circuitry basis that will help further understand the mechanism by which olfactory information-processing in the OB is regulated.

Keywords Centrifugal afferents · Olfactory bulb · Glomerular layer · Neurotropic virus · Trans-synaptic labeling

Introduction

It is evident that attention, emotion, and experience significantly affect perception, learning and memory. Top–down modulation is considered to play a crucial role in influencing the status of the brain [1]. In the olfactory neural system, the most important task is to precisely represent odor information under different brain and behavioral status, such as when sniffing, anesthetized, awake, behaving, and being rewarded [2]. The principles of neuroanatomical structures provide an important reference for how the sensory world is represented in the pattern of neuronal activity [3]. Previous studies have shown the neurons arising from higher cortical regions, including olfactory cortex, send precise top–down projections to different layers of the olfactory bulb (OB), thereby regulating odor perception and olfactory-related learning and memory under different brain and behavioral states [2–6].

Olfactory perception begins at the olfactory mucosa (or olfactory epithelium) in the nasal cavity. Olfactory sensory neurons (OSNs) convert the odor information into electrical signals through binding between odors and receptors

Pengjie Wen and Xiaoping Rao contributed equally to this work.

✉ Xiaobin He
hexb@wipm.ac.cn

✉ Fuqiang Xu
fuqiang.xu@wipm.ac.cn

[1] Center of Brain Science, State Key Laboratory of Magnetic Resonance and Atomic and Molecular Physics, National Center for Magnetic Resonance in Wuhan, Key Laboratory of Magnetic Resonance in Biological Systems, Wuhan Institute of Physics and Mathematics, Center for Excellence in Brain Science and Intelligent Technology, Chinese Academy of Sciences, Wuhan 430071, China

[2] University of the Chinese Academy of Sciences, Beijing 100049, China

[3] College of Life Science, Wuhan University, Wuhan 430072, China

[4] Divisions of Biomedical Photonics, Wuhan National Laboratory for Optoelectronics, Wuhan 430074, China

and send it to the OB, where odorant information is continuously processed by complex local neural circuits and projected to different regions of olfactory cortex [7]. The OB is the first processing center of odor information, where the odorant type, concentration, and constituents are encoded as the spatial and temporal response characteristics of various neurons to facilitate decoding in the olfactory cortex [8]. In consequence, the OB plays the most critical role in odor threshold, odor discrimination, and odor-related learning and memory [9]. Apart from transmitting information to the higher cortex, the OB also receives dense innervation from higher brain areas, including feedback and centrifugal inputs [3, 5, 7]. The projections from piriform cortex (Pir) and the anterior olfactory nucleus (AON) are the major source of feedback inputs [3], and the centrifugal inputs include cholinergic, noradrenergic, and serotonergic modulation [5]. Specific manipulation of the circuits by optogenetics has revealed that all these projections dramatically modulate the cellular activity and neural circuits involved in odor information-processing and representation in the OB, and affect olfactory-related behaviors [10]. In the past decade, the influence of centrifugal inputs on the coding and perception of odor information has been the frontier of olfactory research [11–15]. However, one of the defects in our understanding of the structure and function of centrifugal input is the lack of comprehensive and accurate structural network information. The network evidence mainly comes from anterograde labeling of projections at the olfactory cortex or modulatory nuclei, while retrograde labeling from the OB is rare [11, 12, 16, 17]. Furthermore, the traditional study of centrifugal input networks is mainly focused on the granule cell layer (GCL) [7], ignoring other layers, especially the glomerular layer (GL), where the axons of OSNs transmit odorant information to the dendrites of mitral/tufted cells (M/TCs) in the OB [7]. In addition, similar to deep short-axon cells (dSACs) and granule cells (GCs) in the GCL, periglomerular cells (PGCs) and superficial short-axon cells (sSACs) in the GL exhibit stronger odor-evoked excitation in the awake state than in the anesthetized state [18], suggesting that centrifugal inputs to the GL significantly modulate their activity across distinct brain states [19].

However, systematically understanding the mechanism of top–down regulation of the different layers of the OB require dissecting the structural organization of the top–down olfactory circuit at the whole-brain scale, along with fine information on the neuronal circuit architecture [20]. Although previous neuroanatomical research, such as tracing with wheat germ agglutinin and horseradish peroxidase, has identified the basic brain regions that give rise to the centrifugal innervation to the OB [21], the fine architecture of these circuits across the whole brain remains to be elucidated. The recent advance in tracing techniques that use engineered neurotropic viruses for trans-synaptic tracing has driven rapid progress in the dissection of neural circuits [22, 23], because of their reduced virulence and restricted trans-synaptic transport in the anterograde and retrograde directions [24].

Therefore, in the present study, we used monosynaptic and trans-synaptic recombinant neurotropic viral tracers separately to dissect the architecture of the top–down regulatory circuits that directly and indirectly innervate the GL of the OB. In the first set of experiments, two kinds of monosynaptic retrograde rabies virus (RV-ΔG-eGFP and RV-ΔG-dsRed, respectively) were injected into the GL and GCL to quantify and compare the distribution and extent of the topographically organized direct projections in the whole brain. In the second set of experiments, the GL was targeted with injections of RV-ΔG-eGFP or pseudorabies virus (PRV531) to determine the distribution of first- and higher-order projections in the whole brain. The results showed that GCL received more direct centrifugal projections, and GL also received direct centrifugal inputs, but only including AON, anterior piriform cortex (APC) and horizontal limb of diagonal band of Broca (HDB). In addition, the neural circuits in the GL of the lateral OB received varied indirect inputs from bilateral cortical neurons in the AON, Pir, Amygdala (AM), Entorhinal cortex (Ent), hippocampus (Hip) and almost all modulatory nuclei. In all, our results suggested that cortical neurons in these regions have considerable reciprocal connections and innervate the neural circuits in GL of the OB to coordinate and regulate the processing of olfactory information.

Materials and Methods

Animals

Twenty male adult C57 mice (8–10 weeks old, purchased from the Animal Center of Zhongnan Hospital of Wuhan University, Wuhan, China) were housed in a specific pathogen-free facility at a controlled room temperature (22 ± 2 °C) with 60%–80% humidity, under a 12 h:12 h light/dark cycle. Food and water were available *ad libitum*. During experiments, animals that received viral inoculations were then housed and perfused in Biosafety Level-II animal facilities at the Wuhan Institute of Physics and Mathematics.

Rabies Virus Injection

The recombinant tracers RV-ΔG-eGFP and RV-ΔG-dsRed were prepared by BrainVTA (Wuhan, China). Animals were anesthetized with chloral hydrate (400 mg/kg), and

then placed in a stereotaxic apparatus (RWD, Shenzhen, China). During surgery and virus injection, anesthesia was maintained with isoflurane (1%). RV-ΔG-eGFP and RV-ΔG-dsRed (80 nL, 1×10^9 plaque-forming units pfu/mL) were simultaneously injected (50 nL/min) respectively into the ventrolateral GL and ventromedial GCL. The GL coordinates were 4.7 mm anterior to bregma, 1.35 mm from the midline, and 1.75 mm ventral to the dura. The GCL coordinates were 4.7 mm anterior to bregma, 0.7 mm from the midline, and 1.75 mm ventral to the dura. Eight days after virus infection, the animals were transcardially perfused with physiological saline followed by 4% paraformaldehyde (PFA).

PRV531 Injection

The recombinant tracer PRV531 was prepared by BrainVTA. Animals were anesthetized with chloral hydrate (400 mg/kg) and fixed in a stereotaxic instrument (Stoelting, Illinois, USA). The recombinant tracer PRV531 (120 nL, 2×10^9 pfu/mL) was injected (50 nL/min) into the GL. At 48 h and 72 h after virus infection, the animals were transcardially perfused with physiological saline followed by 4% PFA.

Tissue Section Preparation, Imaging, and Data Analysis

The brain was removed, post-fixed in PFA overnight, dehydrated in 30% (w/v) sucrose for 3 days, and then sectioned coronally on a cryostat microtome (NX50, Thermo, Massachusetts, USA). The sequential whole-brain sections, 40 μm thick, were transferred into 24-well plates for storage at − 20 °C. For florescent imaging, they were wet-mounted DAPI, sealed with nail polish, and imaged with TCS SP8 fluorescence laser scanning confocal microscope (Leica, Wetzlar, Germany) or the VS120 virtual microscopy slide-scanning system (Olympus, Tokyo, Japan). The acquired images were adjusted with NIS-Elements Viewer 4.0 (Nikon, Tokyo, Japan), and processed with Adobe Photoshop CS4 and Adobe Illustrator CS6.0 for illustrations. For cell counting, the boundaries of brain regions were delineated manually with Photoshop based on the Allen Brain Atlas and the Mouse Brain Atlas (Fourth Edition). The labeled neurons were counted manually. The data in Rabies Virus cases are presented as the percentage of the total number of labeled neurons in the OB, AON, and HDB, and the numbers of labeled neurons in the anterior piriform cortex (APC) and posterior piriform cortex (PPC) were also counted. For statistical analyses, we examined the distribution of the raw data using the Kolmogorov-Smirnov test in SPSS (version 13.0). Then we used the independent-samples *t* test to determine if the data were normally distributed, and the statistical significance was set at $***P < 0.001$, $**P < 0.01$, and $*P < 0.05$. All values are presented as mean ± SEM. Graphs were drawn using Origin 9.0.

Results

Tracing the Local Circuits Within the OB

To systematically dissect the organization of the top–down olfactory circuits, the injection of viral tracer was well localized to the GL and GCL (Fig. 1A, F). In the cases of RV-mediated retrograde labeling from the GL and GCL (Fig. 1A–E), the RV-labeled neurons were mainly distributed on the ipsilateral side and scattered from the GL to the GCL, especially in the mitral cell layer (MCL) (Fig. 1B–D), indicating that local neural circuits communicate information from almost every layer in the OB to the GL and GCL. In the case of RV-ΔG-dsRed-mediated retrograde labeling from the GCL, most of the labeled neurons were in the local GCL specifically (GL: 4.86% ± 2.80%; external plexiform layer or EPL: 16.62% ± 4.35%; MCL: 21.72% ± 4.33%; internal plexiform layer or IPL: 10.34% ± 2.01%; GCL: 46.43% ± 11.15%) (Fig. 1B–E). Quantitative analysis showed that the main population of RV-ΔG-eGFP-mediated retrograde labeling from the GL was in the local GL (GL: 53.20% ± 9.55%; EPL: 16.12% ± 3.98%, MCL: 6.47% ± 2.44%; IPL: 15.25% ± 2.96%; GCL: 4.55% ± 2.20%) (Fig. 1B–E). In addition, neurons in the contralateral OB did not show retrograde labeling by RV, indicating that there was no direct neural projection to the contralateral GL and GCL (Fig. 1D), because only neurons with somata and axon terminals at the injection site can be labeled by glycoprotein-deleted RV [3, 25].

In the PRV-mediated retrograde and trans-synaptic tracing, the injection of virus was limited to the range of 5–10 glomeruli in the GL (Fig. 1F, G); this is the first subregion for olfactory information processing. At the early stage of infection (after 48 h), the trans-synaptically infected local neural circuits were distributed across the ipsilateral OB, scattering from the GL to the GCL (Fig. 1G, H). The labeled circuits were organized in column-like structures (Fig. 1H), consistent with previous reports [26]. Meanwhile, a few neurons were labeled on the other side of the injected OB, but not in the contralateral OB (Fig. 1G, H). With extension of the infection time to 72 h, the local circuit of the injected OB was densely labeled and exhibited column-like structures (Fig. 1I, J). Neurons in the contralateral OB were also labeled (Fig. 1J), indicating that the bilateral OBs are indirectly connected to each other.

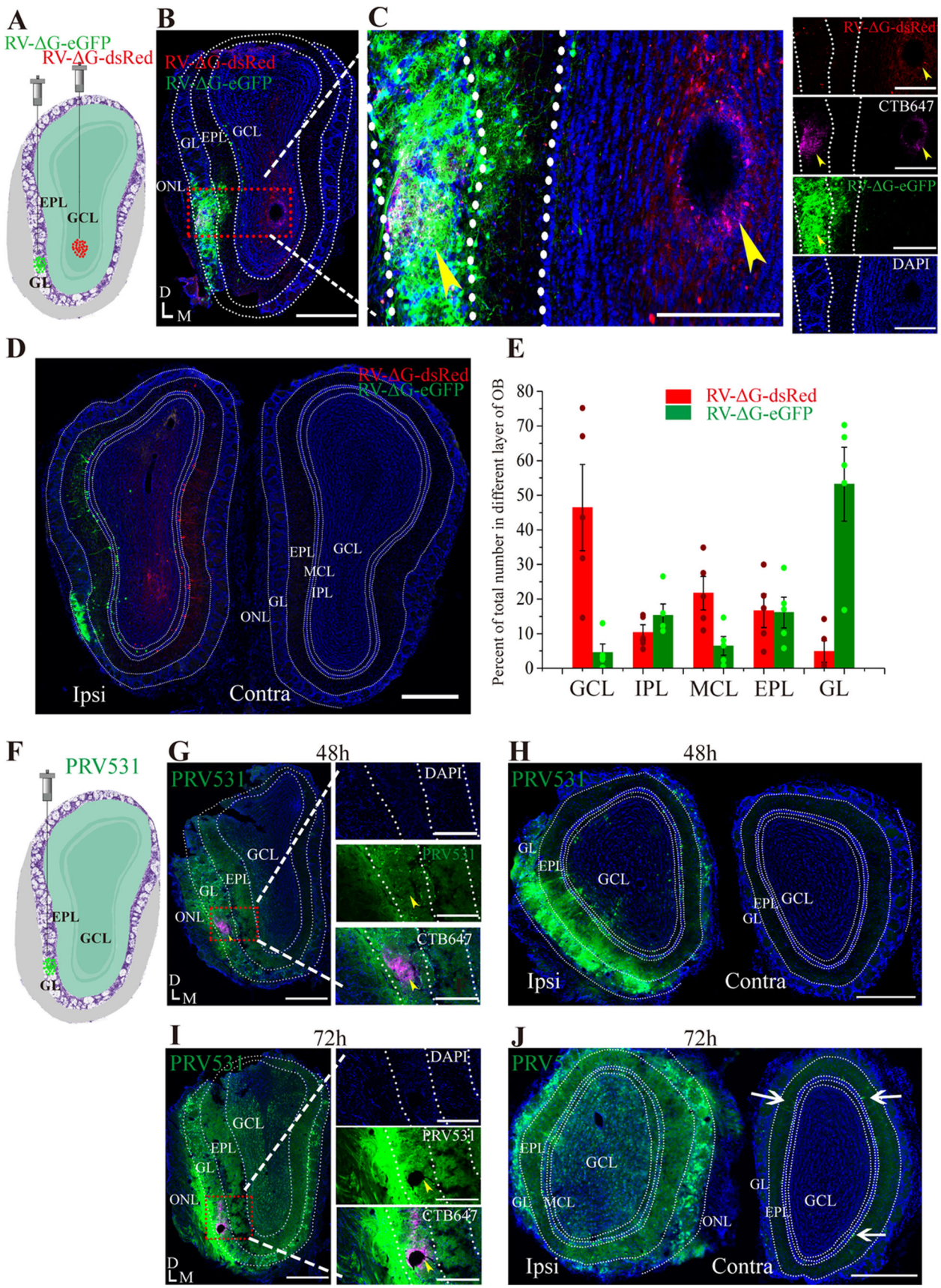
A
RV-ΔG-eGFP
RV-ΔG-dsRed
EPL
GCL
GL
B
RV-ΔG-dsRed
RV-ΔG-eGFP
GL
EPL
GCL
ONL
D
M
C
RV-ΔG-dsRed
CTB647
RV-ΔG-eGFP
DAPI
D
RV-ΔG-dsRed
RV-ΔG-eGFP
EPL
GCL
MCL
IPL
GL
ONL
Ipsi
Contra
E
RV-ΔG-dsRed
RV-ΔG-eGFP
Percent of total number in different layer of OB
80
70
60
50
40
30
20
10
0
GCL
IPL
MCL
EPL
GL
F
PRV531
EPL
GCL
GL
G
48h
PRV531
GCL
EPL
GL
ONL
D
M
DAPI
PRV531
CTB647
H
48h
PRV531
GL
EPL
GCL
EPL
GCL
GL
Ipsi
Contra
I
72h
PRV531
GCL
EPL
GL
ONL
D
M
DAPI
PRV531
CTB647
J
72h
PRV5
EPL
GCL
GL
MCL
ONL
GL
EPL
GCL
Ipsi
Contra

◀**Fig. 1** Organization of retrogradely-labeled neurons in the OB. **A** Schematic outlining the experimental design for RV-mediated retrograde labeling in the GL and GCL of the OB. **B** Injection sites of RV-ΔG-dsRed (red) and RV-ΔG-eGFP (green), each simultaneously injected into the GCL and GL of the OB along with dye (CTB647, pink) (scale bar, 100 μm). **C** Enlargements of B, arrowheads indicate sites of injection. **D** Only the ipsilateral OB had areas of retrogradely-labeled neurons (red and green) in the GL, EPL, MCL, IPL and GCL. **E** Ratios of RV-mediated infected neurons in each layer of the ipsilateral OB. **F** Schematic outlining the experimental design for PRV-mediated retrograde labeling in the GL. **G**, **I** Injection sites (arrowheads) of PRV531 (green) and dye (CTB647, pink). **H**, **J** Patterns of PRV-mediated trans-synaptic labeling of neurons in the bilateral OB at 48 h (H) and 72 h (J) after injection into the GL. Arrows indicate contralateral M/TCs infected by PRV 72 h after injection. Contra, contralateral; D, Dorsal; EPL, external plexiform layer; IPL, internal plexiform layer; MCL, mitral cell layer; GCL, granule cell layer; GL, glomerular layer; M, medial; Ipsi, ipsilateral; ONL, olfactory nerve layer. Scale bar, 500 μm; **C**, **G**, **I** insets 250 μm, $n = 5$.

Circuits in the AON Project to the OB

The AON is considered to be responsible for the processing of olfactory information related to direction and concentration through the feedback projections to the bilateral OBs and reciprocal projections between the bilateral AONs [27, 28]. In the case of RV-mediated retrograde tracing, neurons of the AON and anterior olfactory area external part (AOE) were labeled uniformly by both RV-ΔG-eGFP and RV-ΔG-dsRed from the GL and GCL respectively (Fig. 2A, B). In all, the dsRed-positive neurons were distributed in the bilateral AON and AOE, with the majority in the ipsilateral (Ipsi, 70.88% ± 1.15%; Contra, 27.58% ± 0.86%; $t = 30.10$, $P < 0.001$, $n = 4$), whereas the GFP-positive neurons (Ipsi, 1.28% ± 0.40%; Contra, 0.26% ± 0.13%) were much fewer than those with dsRed (Ipsi, $t = 56.97$, $P < 0.001$; Contra, $t = 31.36$, $P < 0.001$; $n = 4$) and were mostly in the ipsilateral too ($t = 2.41$, $P = 0.08$, $n = 4$) (Fig. 2A–C, F). These results indicated that neurons in the AON and AOE send direct feedback projections to the bilateral GCL and GL of the OB, but more to the GCL and the ipsilateral.

In the PRV-mediated retrograde and RV tracing from the GL of the OB, the distribution of PRV GFP-positive neurons in the bilateral AON and AOE was more denser than that of RV tracing (Fig. 2C, D, F, G), indicating that it crossed more synapses and more neurons were labeled by PRV 48 h after injection than by RV. In addition, at both 48 h (Fig. 2D, G) and 72 h after infection (Fig. 2E, H), the density of the distribution of GFP-positive neurons was comparable in the bilateral AON and AOE, and all subregions of the bilateral AON had similar GFP levels (Fig. 2D, E, G, H). This result showed that there are strong reciprocal projections between the bilateral AON and AOE, consistent with the previous report [27].

Circuits in the Piriform Cortex Project to the OB

The APC is considered to encode information related to the structural or perceptual identity of an odor [29]. In the case of RV-mediated retrograde tracing, the labeled neurons were mainly distributed in layers II and III of the ipsilateral APC (I, 2.44 ± 0.73; II, 147.46 ± 11.08; III, 68.55 ± 15.61) (Fig. 3A–C). The number of dsRed- positive neurons in layer II was double that in layer III (Fig. 3C). In addition, the number of eGFP-positive neurons (I, 0; II, 10.28 ± 7.11; III, 7.43 ± 3.22) was much lower than that of the dsRed-positive neurons in each layer (II, $t = 10.42$, $P < 0.0001$; III, $t = 3.83$, $P = 0.02$; $n = 3$) (Fig. 3A, C). These results indicated that the main feedback projections from the APC are in the GCL of the ipsilateral OB. In addition, there were weak feedback projections from APC to the GL, which have not been reported previously.

The PPC encodes the perceptual category of an odor, such as 'fruity' [29]. In the case of RV-mediated retrograde tracing, the labeled neurons were mainly distributed in layers II and III of the ipsilateral PPC, similar to the APC (Fig. 4A–C). The dsRed-positive neurons were mainly located in layer II (64.21 ± 14.68), where the number was double that in layer III (29.75 ± 4.81) ($P = 0.09$, $n = 3$) (Fig. 4C). Meanwhile, eGFP-positive neurons were not observed in the PPC (Fig. 4B). These results indicated a main feedback projection from the PPC to the GCL of the ipsilateral OB.

In the APC and PPC, the GFP-positive neurons in the PRV-mediated retrograde and trans-synaptic tracing from the GL of the OB were mainly distributed in layers II and III at the earlier stage of infection (48 h after infection) (Figs. 3E and 4G). The distribution density of GFP-positive neurons in the ipsilateral APC/PPC was higher than that in the contralateral APC/PPC (Figs. 3E, H and 4G, J). With the prolongation of infection (72 h after infection), the distribution density of GFP-positive neurons increased significantly, especially in layers II and III of the bilateral APC/PPC (Figs. 3F, I and 4H, K).

Circuits in the Amygdala Project to the OB

The AM has long been known to play critical roles in the processing and retrieval of emotions, such as fear, reward, and happiness [30]. The nuclei of the AM receive direct projections from the OB and AOB [31]. In the case of RV-mediated retrograde tracing, dsRed-positive neurons were mainly located in the ipsilateral basomedial AM (Fig. 4D, E), but no neurons were labeled by RV-dG-eGFP from the GL of the OB in the bilateral AM (Fig. 4D–F, I). In the PRV-mediated retrograde and trans-synaptic tracing, the GFP-positive neurons were mainly distributed in the

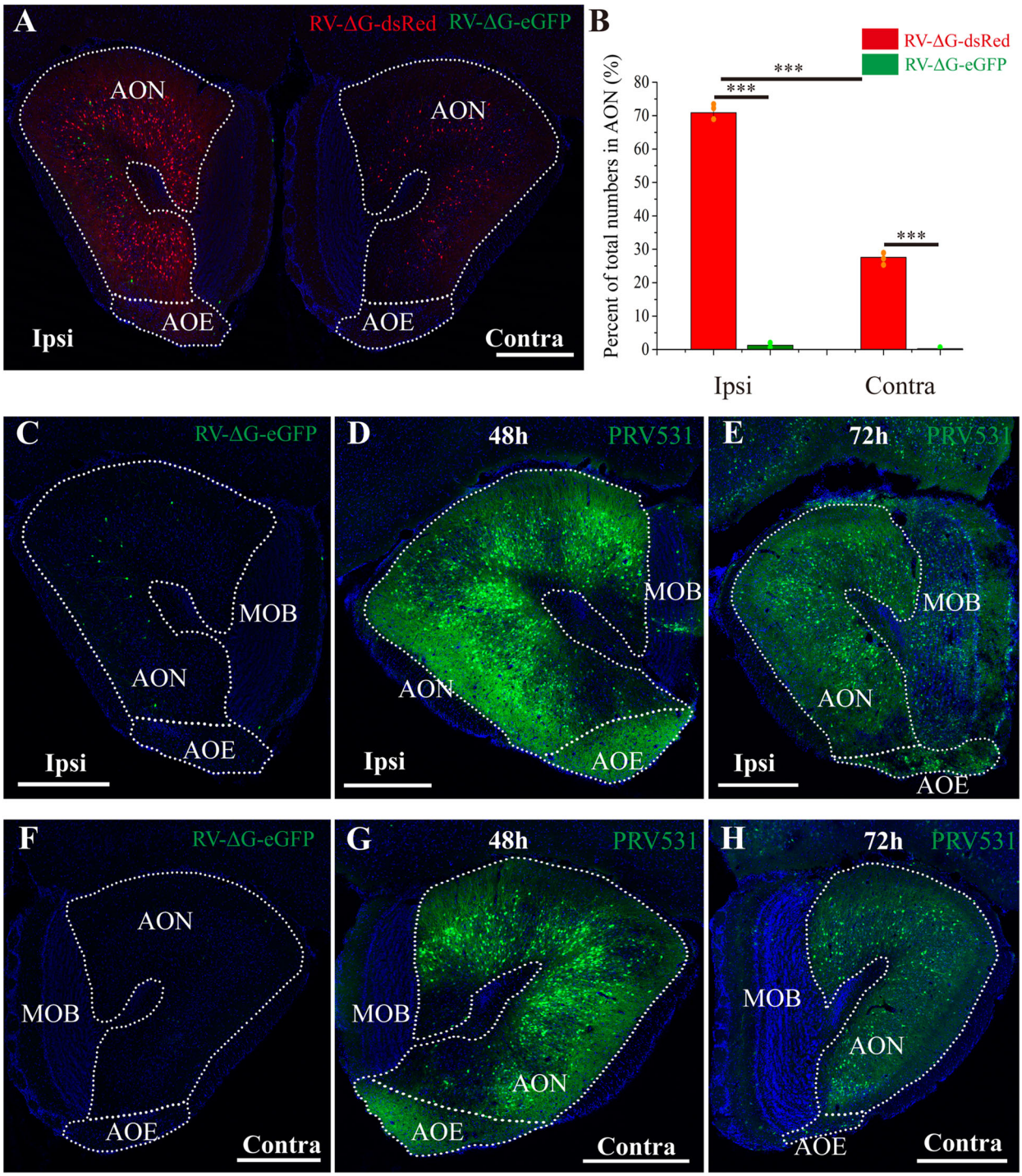

Fig. 2 Organization of retrogradely-labeled neurons in the anterior olfactory nucleus (AON) and the anterior olfactory area external part (AOE). **A** Neurons in the bilateral AONs (including AOEs) infected by RV-ΔG-dsRed (*red*) and RV-ΔG-eGFP (*green*) injected into the GCL and GL of OB respectively. **B** Ratios of all RV-mediated infected neurons in the bilateral AONs (***$P < 0.001$, independent-samples *t* test). **C**–**E** Neurons in the ipsilateral AON and AOE labeled by RV-ΔG-eGFP (**C**) and PRV531, the latter at 48 h (**D**) and 72 h (**E**) after injection into the GL of the OB. **F**–**H** Neurons in the contralateral AON and AOE labeled by RV-ΔG-eGFP (**F**) and PRV531, the latter at 48 h (**G**) and 72 h (**H**) after injection into the GL of the OB. MOB, main olfactory bulb; scale bar, 500 μm; $n = 4$.

ipsilateral basomedial AM and basolateral ventral AM at the early stage of infection (48 h after infection) (Fig. 4G). By 72 h after infection, the density of PRV GFP-positive neurons increased across the subregions of the AM, including the basomedial, basolateral ventral, and basolateral amygdala, posterodorsal and posteroventral subnuclei

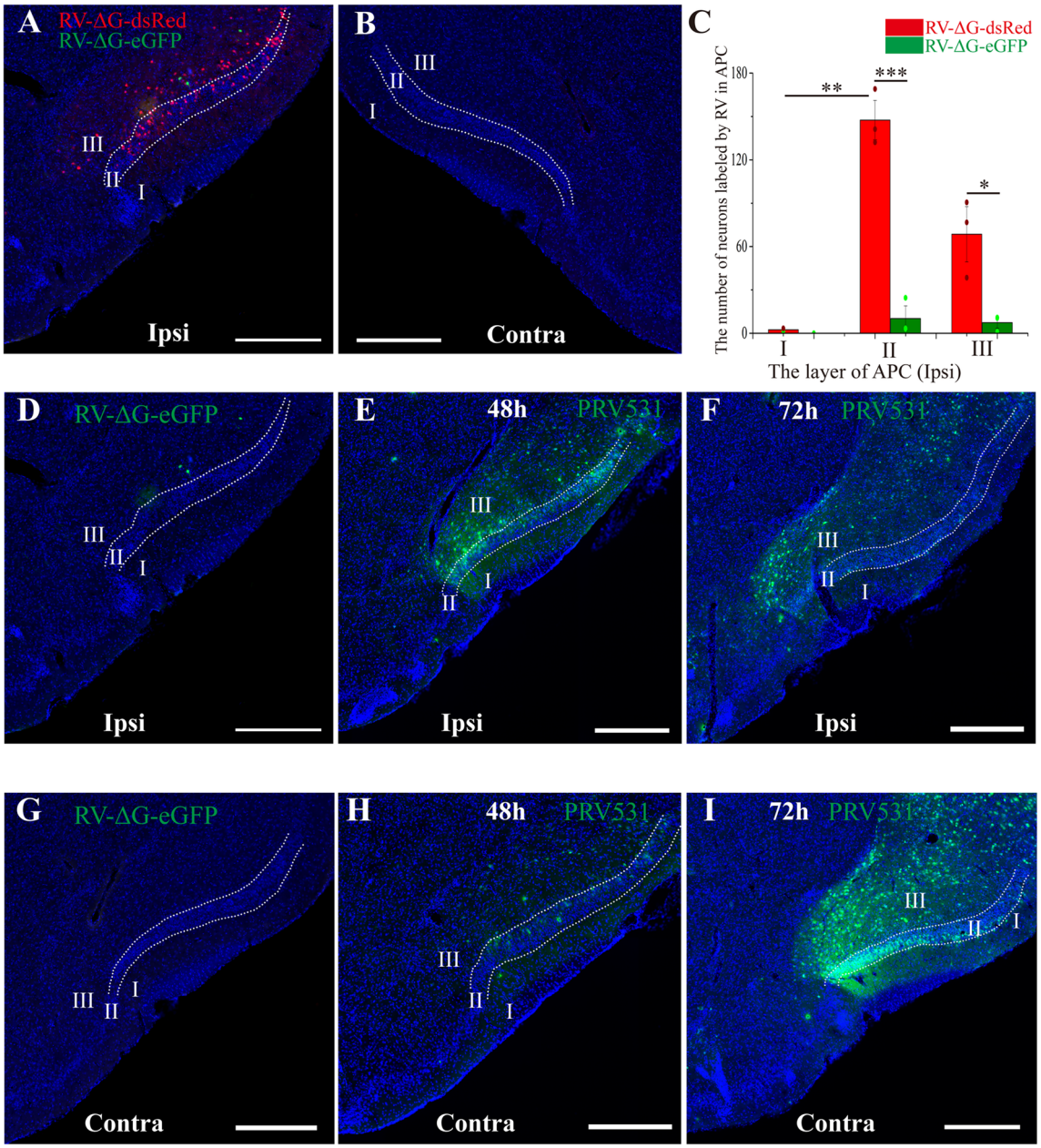

Fig. 3 Organization of retrogradely-labeled neurons in the anterior piriform cortex (APC). **A** Neurons in layers II and III of the ipsilateral APC infected by RV-ΔG-dsRed (*red*) and RV-ΔG-eGFP (green), injected into the GCL and GL, respectively. **B** There were no labeled neurons in the contralateral APC in both RV-mediated cases. **C** Numbers of RV-mediated infected neurons in different layers of the ipsilateral APC. There were more dsRed-positive than eGFP-positive neurons, and the number of labeled neurons in layer II was double that in layer III in the dsRed-positive case. $***P < 0.001$, $**P < 0.01$, $*P < 0.05$, independent-samples *t* test. **D–F** Neurons in the ipsilateral APC labeled by RV-ΔG-eGFP (**D**) and PRV531, the latter at 48 h (**E**) and 72 h (**F**) after injection into the GL of the OB. **G–I** Neurons in the contralateral APC labeled by RV-ΔG-eGFP (**G**) and PRV531, the latter at 48 h (**H**) and 72 h (**I**) after injection into the GL of the OB. Scale bars, 500 μm; $n = 3$.

of the medial AM, and the posteromedial and posterolateral cortical AM (PLCo) (Fig. 4H). In addition, no neuron showed retrograde labeling in the contralateral AM at the early stage (48 h) of infection(Fig. 4I, J), and there were fewer GFP-positive neurons scattered in the contralateral subregions and subnuclei of the AM at 72 h than on the ipsilateral side (Fig. 4K).

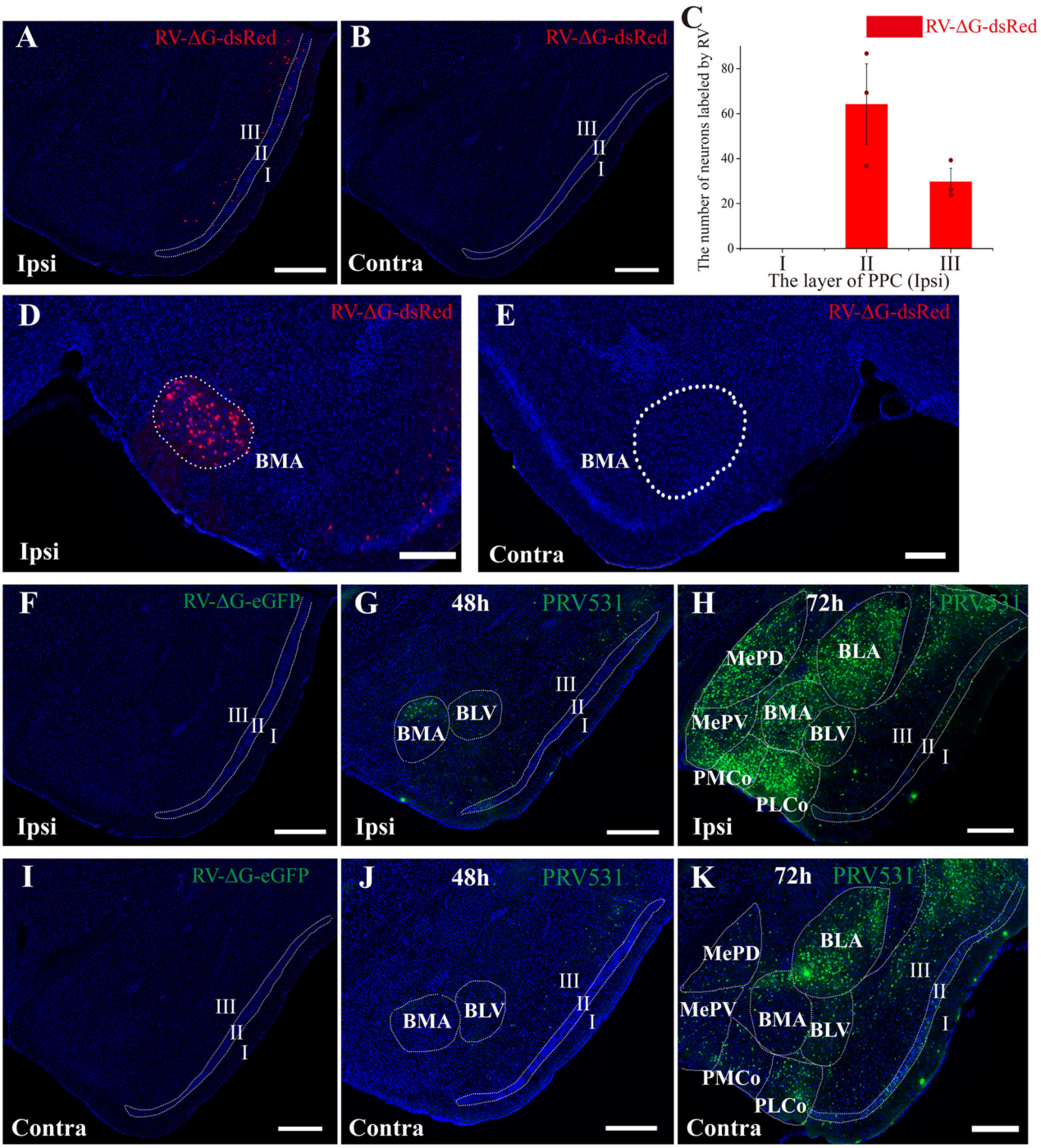

Fig. 4 Organization of retrogradely-labeled neurons in the poster piriform cortex (PPC) and amygdala (AM). **A** Neurons in the layers II and III of the ipsilateral PPC infected only by RV-ΔG-dsRed (red) injected into the GCL of the OB, and not by RV-ΔG-eGFP (green) from the GL. **B** There were no labeled neurons in the contralateral PPC in both RV-mediated cases. **C** Numbers of RV-mediated infected neurons in different layers of ipsilateral PPC. The number of dsRed-positive neurons in layer II was double that in layer III. No eGFP-positive neurons were found in the PPC (independent-samples *t* test). **D** Neurons in the ipsilateral AM infected only by RV-ΔG-dsRed (red) injected into the GCL of the OB, and not by RV-ΔG-eGFP (green) from the GL. **E** There were no labeled neurons in the contralateral AM in both RV-mediated cases. **F**–**H** Neurons in the ipsilateral PPC and AM labeled by RV-ΔG-eGFP (F) and PRV531, the latter at 48 h (**G**) and 72 h (**H**) after injection into the GL of the OB. **I**–**K** Neurons in the contralateral PPC and AM labeled by RV-ΔG-eGFP (**I**) and PRV531, the latter at 48 h (**J**) and 72 h (**K**) after injection into the GL of the OB. BLA, basolateral amygdala; BLV, basolateral amygdaloid ventral; BMA, basomedial amygdala; MePD, medial amygdaloid posterodorsal; MePV, medial amygdaloid posteroventral; PLCo, posterolateral cortical amygdale; PMCo, posteromedial cortical amygdala. Scale bars, 250 μm; $n = 3$.

Circuits in the Entorhinal Cortex (Ent) and Hippocampus (Hip) Project to the OB

Previous studies have reported that the Ent not only receives inputs from the OB, PC, medial AM and Hip, but also sends feedback projections to the OB, PC, and Hip [32, 33]. This special circuit may allow the Ent to regulate olfactory coding based on memory, experience, and preference [33]. In this study, RV-ΔG-dsRed neurons labeled by retrograde tracing were only found in the ipsilateral Ent (94 ± 24.11) and CA1 (29.8 ± 6.16) (Fig. 5A, B), suggesting that the Ent and Hip have direct feedback projections to the GCL of the ipsilateral OB. The number of dsRed-positive neurons in the Ent was 3–4 times higher than that in CA1, although the difference did not reach significance ($t = 2.58$, $P = 0.054$, $n = 5$) (Fig. 5C).

In PRV-mediated retrograde and trans-synaptic tracing from the GL of the OB, GFP-positive neurons were mainly distributed in the bilateral Ent and CA1 at 48 h after infection (Fig. 5D, F), and 72 h after infection, the density of PRV GFP-positive neurons increased significantly in the bilateral Ent, Hip, and peripheral areas, including the CAl/2/3 fields of the Hip, dentate gyrus, amygdalopiriform transition area, PMCo, basolateral posterior AM, perirhinal

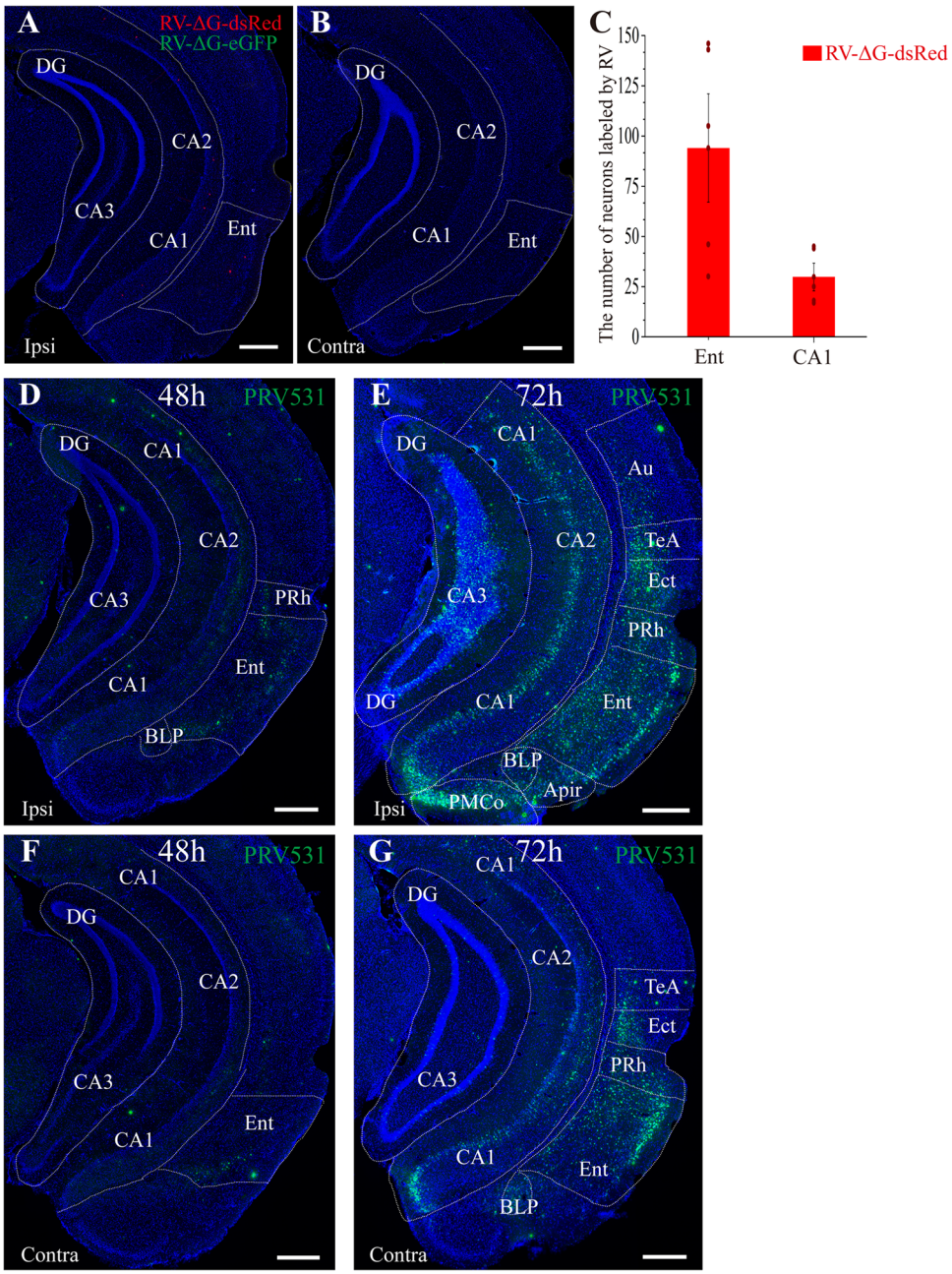

Fig. 5 Organization of retrogradely-labeled neurons in the entorhinal cortex (Ent) and hippocampus (Hip). **A** Neurons in the ipsilateral Ent and CA1 infected only by RV-ΔG-dsRed (red) injected into the GCL of the OB, not by RV-ΔG-eGFP (green) from the GL. **B** No neurons were labeled in the contralateral Ent and Hip in both RV-mediated cases. **C** Numbers of RV-mediated infected neurons in the ipsilateral Ent and CA1 (independent-samples *t* test). **D–E** Neurons in the ipsilateral Ent and Hip areas labeled by PRV531 at 48 h (**D**) and 72 h (**E**) after injection into the GL of the OB. **F–G** Neurons in the contralateral Ent and Hip labeled by PRV531 at 48 h (**F**) and 72 h (**G**) after injection into the GL of the OB. APir, amygdalopiriform transition area; Au, primary auditory cortex; BLP, basolateral amygdala, posterior; DG, dentate gyrus; Ect, ectorhinal cortex; PMCo, posteromedial cortical amygdala; PRh, perirhinal cortex; TeA, temporal association cortex. Scale bar, 500 μm; $n = 5$.

cortex, ectorhinal cortex, temporal association cortex, and primary auditory cortex (Fig. 5E, G).

Neuromodulatory Circuits Project to the OB

In addition to receiving intensive feedback projections from olfactory-related cortex, the OB also receives neuromodulatory centrifugal projections from neurons that release acetylcholine, serotonin, and norepinephrine; these projections are also necessary for the brain to regulate the processing of olfactory information [5]. In this study, the RV-mediated retrograde tracing showed that the ipsilateral HDB was labeled by both RV-ΔG-dsRed and RV-ΔG-eGFP (Fig. 6A, B, E, H). The percent of dsRed-positive neurons (80.27% ± 0.33%) was five-fold that of eGFP-positive neurons (16.51% ± 0.80%; $t = 73.80$, $P < 0.0001$, $n = 4$) (Fig. 6B). Besides, a small group of neurons expressed both dsRed and eGFP ($t = 9.71$, $P < 0.0001$ eGFP-positive *versus* merged; $n = 4$) (Fig. 6A, B). These results suggested that axons of cholinergic neurons from the ipsilateral HDB project mainly to the GCL, while project to both the GCL and the GL. In the dorsal raphe (DR) and ipsilateral locus coeruleus (LC), only sparsely distributed dsRed-positive neurons were observed (Fig. 6C, D), suggesting that the axons of both norepinephrinergic and serotoninergic neurons project weakly to the GCL. There was no fluorescence in the median raphe (MR) nucleus (data not shown).

In the PRV-mediated retrograde and trans-synaptic tracing from the GL of the OB, the GFP-positive neurons were mainly distributed in the bilateral HDB and LC at the early stage of infection (48 h), and the distribution of PRV GFP-positive neurons in the ipsilateral HDB and LC was significantly more prominent than that in the contralateral HDB and LC (Fig. 6F, I, M). After infection for 72 h, the density of PRV GFP-positive neurons was significantly higher in the DR and MR, and bilaterally in the HDB and LC (Fig. 6F–G, I–N), and even extended to peripheral nuclei, such as the lateral nucleus of the diagonal band (Fig. 6G, J, L, N).

Discussion

By combining monosynaptic RV-mediated tracing with PRV-mediated trans-synaptic retrograde labeling, we have described the cortical organization of centrifugal afferents to the GL and GCL of the OB (Fig. 7). We first compared the brain regions directly projecting into the GL and GCL, which indicated that the GL only received inputs from each layer in the OB and centrifugal inputs from the ipsilateral AON, APC, and the HDB (Fig. 7A). Retrograde tracing with PRV531 at two time points after viral infection (48 h and 72 h) uncovered various organizational patterns of the neurons that give rise to direct or indirect innervations of the neural circuits in the GL of the lateral OB. At 48 h post-infection, trans-synaptic GFP-labeled neurons were sparsely distributed in the bilateral AON, Pir, AM, Ent, Hip, HDB, LC, DR, and MR (Fig. 7B). At 72 h post-infection, a marked increase in the number of GFP-labeled neurons was found in these olfactory-related cortical regions and neuromodulatory nuclei (Fig. 7C). These results showed that the neural circuits of the GL in the lateral OB receive both direct and indirect feedback and centrifugal inputs, which will help to further understand how olfactory information processing is regulated in the OB.

Local Intra-bulbar Microcircuits

With RV-mediated labeling from the GL, infected neurons were distributed throughout the GL, EPL, MCL, IPL, and GCL. In the GL, especially within each glomerulus, OSN terminals excite the apical dendritic tufts of tens of homotypic M/TCs [34, 35] and various juxtaglomerular cells [glutamatergic external tufted cells (ETCs), GABAergic periglomerular cells (PGCs), and combined GABAergic and dopaminergic superficial short-axon cells (sSACs)] [19, 36, 37]. ETCs provide the principal excitatory drive to MCs and the entire glomerular microcircuit, composed of PGCs and sSACs [35, 38]. GABA release from PGCs mediates glomerulus-wide suppression of homotypic M/TCs through direct gap-junctional coupling between homotypic PGCs [39–41]. The majority of sSACs, which mediate robust monosynaptic GABAergic inhibitory signaling in ETCs and M/TCs by gap-junctional coupling somatodendritic contacts with local sSACs [36, 42], may support distinct scales of interglomerular interactions due to multiple axonal branch projections of distant sSACs even up to several tens of glomeruli [37, 43]. Together, these neurons form local microcircuits in the GL. MC and TC somata are arrayed in the MCL and throughout the EPL, respectively, while their apical dendritic tufts receive both excitation from OSN terminals and/or ETCs and inhibition from PGCs and/or sSACs [19]. In addition, calbindin-positive PGCs not only receive input from ETCs in the GL, but also from TCs and MCs [40]. These circuits may establish connections from the EPL/MCL to the GL. Moreover, PGCs, ETCs, and TC apical dendrites in the GL, but not MCs, receive inhibitory GABAergic inputs from the GL-projecting deep SACs (dSACs) whose somata are located in the IPL or GCL and whose axons arborize extensively across the GL [44, 45]. Therefore, GL-projecting dSACs, which may participate in multi-glomerular coordination, establish a novel intra-bulbar projection from deep to superficial layers, from the IPL/GCL to the GL.

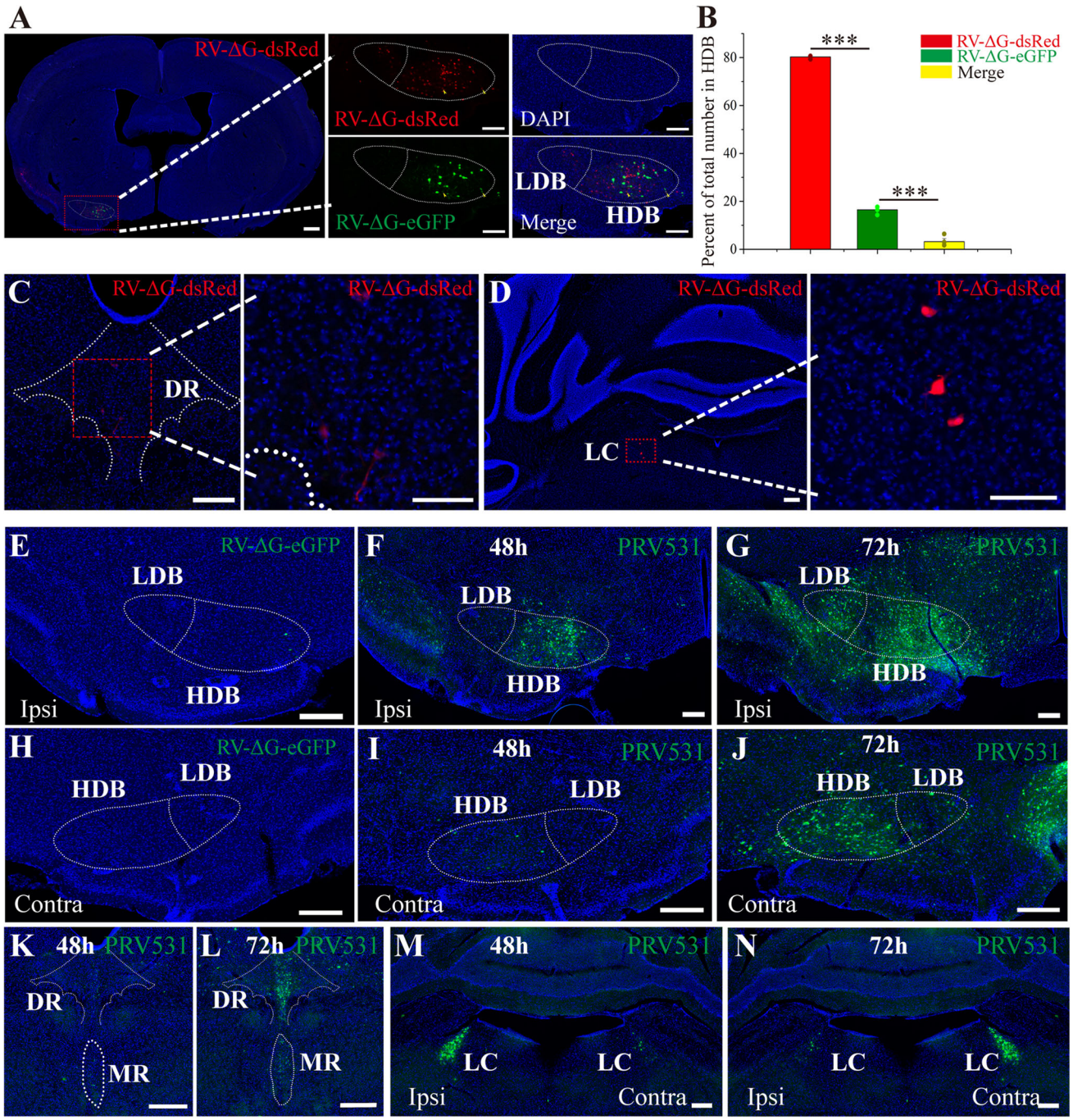

Fig. 6 Organization of retrogradely-labeled neurons in the horizontal limb of the diagonal band of Broca (HDB), dorsal raphe (DR), median raphe (MR), and locus coeruleus (LC). **A** Neurons in the HDB infected by RV-ΔG-dsRed (red) and RV-ΔG-eGFP (green) injected into the GCL and GL of the OB. **B** Statistical analysis of the difference between the numbers of RV-infected neurons in the HDB for the two cases (***$P < 0.001$, independent-samples t test). **C**–**D** Neurons in the DR (**C**) and LC (**D**) only infected by RV-ΔG-dsRed (red) injected into the GCL, and not by RV-ΔG-eGFP (green) injected into the GL. **E**–**J** Neurons in the bilateral HDB labeled by RV-ΔG-eGFP (**E**, **H**) and PRV531, the latter at 48 h (**F**, **I**) and 72 h (**G**, **J**) after injection into the GL. **K**–**L** Neurons in the DR and MR labeled by PRV 531 at 48 h (**K**) and 72 h (**L**) after injection into the GL. **M**–**N** Neurons in the bilateral LC labeled by PRV 531 at 48 h (**M**) and 72 h (**N**) after injection into the GL. Scale bars, 500 μm; **A**, **C**, **D** insets, 250 μm; $n = 4$.

With RV-mediated labeling from the GCL, infected neurons were also distributed throughout the GL, EPL, MCL, IPL, and GCL. There are two kinds of interneuron in GCL: GCs and dSACs; the latter are GABAergic and have extensive axonal ramification in various layers of the OB [45, 46] and they strongly inhibit GCs [45, 46]. It has been

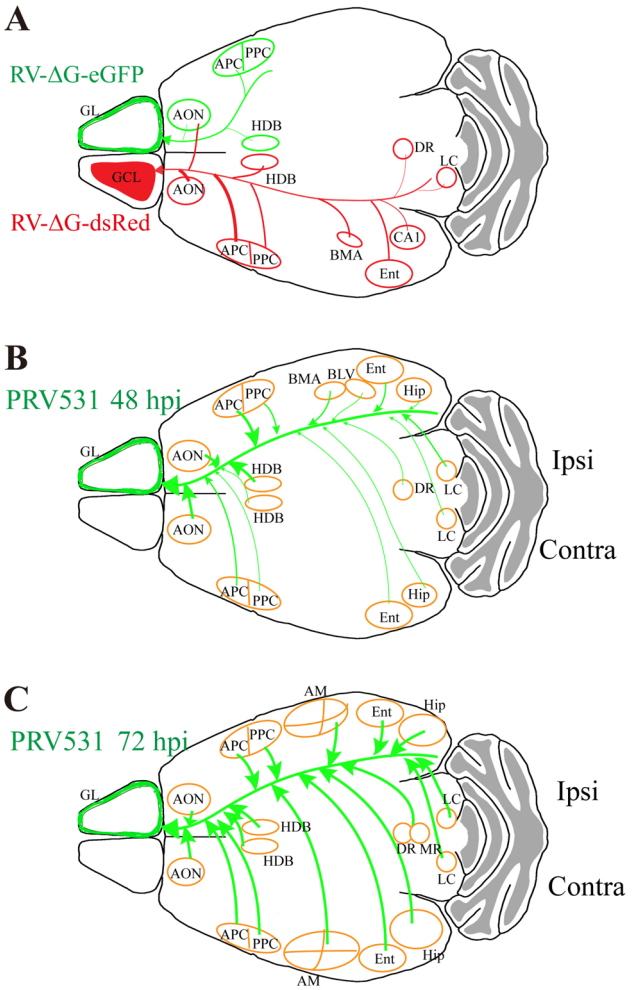

Fig. 7 Cortical organization of centrifugal afferents to the GL of the OB. **A** The GCL receives direct centrifugal inputs from the bilateral AON, ipsilateral APC, PPC, BMA, Ent, CA1, HDB, DR, and LC, but the GL only receives direct centrifugal inputs from the ipsilateral AON, APC, and HDB. **B** PRV531 at 48 h after injection into the GL. Some neurons were labeled in the bilateral AON, APC, PPC, Ent, Hip, HDB, DR, and LC, and the ipsilateral BMA and BLV, which indicate that there are direct and indirect projections to the GL. **C** PRV531 72 h after injection into the GL. More neurons were labeled in the bilateral AON, APC, PPC, AM, Ent, Hip, HDB, DR, MR, and LC. AON, anterior olfactory nucleus; APC, anterior piriform cortex; PPC, posterior piriform cortex; AM, amygdala; Ent, entorhinal cortex; Hip, hippocampus; HDB, horizontal limb of the diagonal band of Broca; DR, dorsal raphe; MR, median raphe; LC, locus coeruleus.

estimated that each EPL- and/or GCL-dSAC innervates on the order of 10^3 GCs, with ~75 EPL-and/or GCL-dSACs converging onto each GC [19, 47]. In the EPL, the apical dendrites of superficial GCs and deep GCs form reciprocal dendrodendritic synapses with lateral dendrites of MCs and TCs in the superficial *versus* deep EPL, respectively [19]. In addition, both GCs and dSACs receive axodendritic excitatory synapses from M/TC axon collaterals in the GCL [45, 48]. These neural circuits potentially establish connections from the MCL and/or EPL to the GCL. The apical dendrites of GCs, which receive excitatory synapses from the axons of ETCs in homologous glomeruli, form inhibitory synapses on the ETCs connected to other homologous ipsilateral glomeruli [49, 50]. Therefore, the excitatory input of ETCs onto the proximal primary axons of GCs establisha potential connection from the GL to the GCL. This may also be the only known pathway linking the dorsal and ventral GL in our PRV-mediated trans-synaptic tracing from the GL, in which some infected neurons were in the dorsal GL and MCL.

Feedback from Olfactory Cortex to the OB

The OB receives dense input from higher brain areas, in which the AON and Pir are the major source of feedback [3]. The AON can be subdivided into the pars externa (AOE) and the pars principalis (AONpP). The latter is further segmented into dorsal, ventral, medial, and lateral regions [51]. The AOE feedback to the bulb has been studied; axons from AOE neurons target mirror-symmetric glomeruli in the contralateral OB, creating a bilateral olfactory map [52]. In contrast, projections from the AONpP are known to target the GCL bilaterally [6]; this is consistent with our RV labeling. Moreover, feedback to the GCL from the ipsilateral AON is uniformly distributed, as we found in this study; but we did not find that projections from the contralateral AON showed a strong ventral bias [3]. This may be because our central injection sites were predominantly in the ventral GCL. In addition, this is the first report that neurons of AONpP and AOE send direct feedback projections to the bilateral GL, indicating that there are more neural circuits from the AON to the OB than originally thought.

Neurons in the AON were more densely infected from the GL with PRV- than RV-mediated trans-synaptic tracing. Which circuit provides the ability to make high strength of the PRV GFP tracing in the bilateral AON? As far as we know, AON send weak feedback projection on the GL of the ipsilateral OB and there was no feedback projection on the contra-lateral GL. The dense feedback projections from the AON to the bilateral GCL [6], and the dense projections from the GCL to the GL within the OB [44, 45], as well as the strong reciprocal projections between the bilateral AONs [53], might explain the high efficiency of PRV GFP-mediated trans-synaptic labeling of the bilateral AON.

Apart from the AON, pyramidal neurons in layers II and III of the APC send robust excitatory centrifugal input to the GCs and dSACs in the GCL [54]. But it had not been reported that centrifugal feedback inputs originating PPC to GCL and GL, whose target neurons and possible functions need to be further identified. In addition,

olfactory-related feedback afferents arise from many sources, including the peri-amygdaloid cortex and amygdala [33], but precise neural connections are rarely reported. This is the first report that the basomedial, basolateral, medial, posteromedial cortical, and posterolateral AM could directly and indirectly regulate olfactory information processing in the GL. Because the medial and posteromedial cortical AM received inputs from the AOB, and the posterolateral cortical AM received inputs from the OB [31], these circuits between main olfactory and vomeronasal cortex may be nodes where main and accessory olfactory information converged and are reciprocally regulated.

The OB receives centrifugal projections from the Ent and Hip [55]. The hippocampal formation, which is anatomically and functionally related to olfactory structures especially in rodents, is essential for olfactory identification and the expression of odor memory representations [56]. Anatomically, the Hip receives olfactory information directly through the medial olfactory tract to the hippocampal rudiment and indirectly through the perforant path from the Ent to the dentate gyrus [56]. Retrograde and anterograde tracing experiments have shown that the Hip projections to OB mainly come from ventral CA1 [57, 58], which is consistent with our RV-mediated labeling. Whether these projections from Ent and Hip to the OB process spatial information for olfactory recognition or are involved in olfactory learning and memory remains to be elucidated.

Neuromodulatory Centrifugal Projections to the OB

In addition to the dense centrifugal feedback projections from higher olfactory-related areas, the OB also receives dense neuromodulatory inputs (cholinergic, noradrenergic, and serotonergic) [5, 13, 14]. Cholinergic input to the OB is provided primarily by the axons of neurons whose cell bodies reside in the HDB in the basal forebrain; this has been implicated in odor discrimination and detection, as well as olfactory learning and memory [4, 5]. Both nicotinic and muscarinic receptors are found in the OB and play crucial and complementary roles in regulating the coherence and sparseness of the OB network output and olfactory behaviors [59, 60]. Although each layer in the OB received cholinergic HDB projections, both the GL and IPL are predominant in the distribution of axonal projections in choline acetyltransferase (Chat-Cre) mice [17, 61], which is inconsistent with our RV-mediated retrograde labeling showing that more neurons innervate the GCL than GL. Perhaps this is because the method used in this study through axon terminal RV absorption is different from measuring the density of axon branches. It may also be that cholinergic neurons have more synapses in the GCL than in the GL. In addition to cholinergic inputs, GCs receive centrifugal GABAergic projections from basal forebrain as well as dSACs [62, 63].

The OB receives significant noradrenergic input from the LC and norepinephrine is involved in olfactory associative learning, as well as odor detection and discrimination [64–66]. Norepinephrine dramatically changes the activity of ETCs and GCs [67–69], which is consistent with the RV labeling from the GCL, but no neurons in the LC were infected in RV-mediated labeling from the GL. It may be that the number of ETCs is much smaller than that of GCs [19]. Besides, the density of axons of dopamine-B-hydroxylase in the GL was much lower than that in the GCL [33].

Serotonergic neurons in the raphe nuclei are involved, *via* their extensive innervation, in a variety of functions including depression, anxiety, sleep-wake cycles, reward, patience in decision-making, and sexual preference [70–76]. Serotonergic projections from the DR and MR densely innervate the OB, where they modulate the initial representation and processing of olfactory information [5, 77, 78]. Almost all types of neurons in the OB are dramatically modulated by serotonin [77, 79–83], the DR mainly projecting to the GCL, and the MR to the GL [78]. In our RV-mediated labeling, only neurons in the DR were infected from the GCL, but neurons in the MR were not infected from the GL. This may be because of the difference between the two labeling methods. It is also possible that the two types of projection differ in function.

Acknowledgements We thank Dr. Lingling Xu (Wuhan Institute of Physics and Mathematics) for maintaining and managing the optical platform. This work was supported by grants from the National Natural Science Foundation of China (31400946, 31671120, 31771197, 31329001, 31771156, 91632303, and 81661148053/H09), the Strategic Priority Research Program of Chinese Academy of Science (XDB32030200), and the National Basic Research Development Program (973 Program) of China (2015CB755600).

Conflict of interest The authors declare that they have no competing financial interests.

References

1. Zhang S, Xu M, Kamigaki T, Hoang Do JP, Chang WC, Jenvay S, *et al.* Selective attention. Long-range and local circuits for top–down modulation of visual cortex processing. Science 2014, 345: 660–665.
2. McIntyre JC, Thiebaud N, McGann JP, Komiyama T, Rothermel M. Neuromodulation in chemosensory pathways. Chem Senses 2017, 42: 375–379.
3. Padmanabhan K, Osakada F, Tarabrina A, Kizer E, Callaway EM, Gage FH, *et al.* Diverse representations of olfactory information in centrifugal feedback projections. J Neurosci 2016, 36: 7535–7545.

4. D'Souza RD, Vijayaraghavan S. Paying attention to smell: cholinergic signaling in the olfactory bulb. Front Synaptic Neurosci 2014, 6: 21.
5. Fletcher ML, Chen WR. Neural correlates of olfactory learning: Critical role of centrifugal neuromodulation. Learn Mem 2010, 17: 561–570.
6. Markopoulos F, Rokni D, Gire DH, Murthy VN. Functional properties of cortical feedback projections to the olfactory bulb. Neuron 2012, 76: 1175–1188.
7. Imai T. Construction of functional neuronal circuitry in the olfactory bulb. Semin Cell Dev Biol 2014, 35: 180–188.
8. Uchida N, Poo C, Haddad R. Coding and transformations in the olfactory system. Annu Rev Neurosci 2014, 37: 363–385.
9. Takahashi H, Ogawa Y, Yoshihara S, Asahina R, Kinoshita M, Kitano T, *et al.* A subtype of olfactory bulb interneurons is required for odor detection and discrimination behaviors. J Neurosci 2016, 36: 8210–8227.
10. Grimaud J, Lledo PM. Illuminating odors: when optogenetics brings to light unexpected olfactory abilities. Learn Mem 2016, 23: 249–254.
11. Oswald AM, Urban NN. There and back again: the corticobulbar loop. Neuron 2012, 76: 1045–1047.
12. Otazu GH, Chae H, Davis MB, Albeanu DF. Cortical feedback decorrelates olfactory bulb output in awake mice. Neuron 2015, 86: 1461–1477.
13. Linster C, Cleland TA. Neuromodulation of olfactory transformations. Curr Opin Neurobiol 2016, 40: 170–177.
14. Lizbinski KM, Dacks AM. Intrinsic and extrinsic neuromodulation of olfactory processing. Front Cell Neurosci 2017, 11: 424.
15. Rothermel M, Wachowiak M. Functional imaging of cortical feedback projections to the olfactory bulb. Front Neural Circuits 2014, 8: 73.
16. Manella LC, Petersen N, Linster C. Stimulation of the locus ceruleus modulates signal-to-noise ratio in the olfactory bulb. J Neurosci 2017, 37: 11605–11615.
17. Case DT, Burton SD, Gedeon JY, Williams SG, Urban NN, Seal RP. Layer- and cell type-selective co-transmission by a basal forebrain cholinergic projection to the olfactory bulb. Nat Commun 2017, 8: 652.
18. Wachowiak M, Economo MN, Diaz-Quesada M, Brunert D, Wesson DW, White JA, *et al.* Optical dissection of odor information processing in vivo using GCaMPs expressed in specified cell types of the olfactory bulb. J Neurosci 2013, 33: 5285–5300.
19. Burton SD. Inhibitory circuits of the mammalian main olfactory bulb. J Neurophysiol 2017, 118: 2034–2051.
20. Luo L, Callaway EM, Svoboda K. Genetic dissection of neural circuits. Neuron 2008, 57: 634–660.
21. Thorne RG, Emory CR, Ala TA, Frey WH, 2nd. Quantitative analysis of the olfactory pathway for drug delivery to the brain. Brain Res 1995, 692: 278–282.
22. Callaway EM. Transneuronal circuit tracing with neurotropic viruses. Curr Opin Neurobiol 2008, 18: 617–623.
23. Nassi JJ, Cepko CL, Born RT, Beier KT. Neuroanatomy goes viral! Front Neuroanat 2015, 9: 80.
24. Bienkowski MS, Wendel ES, Rinaman L. Organization of multisynaptic circuits within and between the medial and the central extended amygdala. J Comp Neurol 2013, 521: 3406–3431.
25. Callaway EM, Luo L. Monosynaptic circuit tracing with glycoprotein-deleted rabies viruses. J Neurosci 2015, 35: 8979–8985.
26. Willhite DC, Nguyen KT, Masurkar AV, Greer CA, Shepherd GM, Chen WR. Viral tracing identifies distributed columnar organization in the olfactory bulb. Proc Natl Acad Sci USA 2006, 103: 12592–12597.
27. Kikuta S, Sato K, Kashiwadani H, Tsunoda K, Yamasoba T, Mori K. From the Cover: Neurons in the anterior olfactory nucleus pars externa detect right or left localization of odor sources. Proc Natl Acad Sci USA 2010, 107: 12363–12368.
28. Esquivelzeta Rabell J, Mutlu K, Noutel J, Martin Del Olmo P, Haesler S. Spontaneous rapid odor source localization behavior requires interhemispheric communication. Curr Biol 2017, 27: 1542–1548 e1544.
29. Wilson DA, Sullivan RM. Cortical processing of odor objects. Neuron 2011, 72: 506–519.
30. Tye KM, Deisseroth K. Optogenetic investigation of neural circuits underlying brain disease in animal models. Nat Rev Neurosci 2012, 13: 251–266.
31. Spehr M, Spehr J, Ukhanov K, Kelliher KR, Leinders-Zufall T, Zufall F. Parallel processing of social signals by the mammalian main and accessory olfactory systems. Cell Mol Life Sci 2006, 63: 1476–1484.
32. Sewards TV, Sewards MA. Input and output stations of the entorhinal cortex: superficial vs. deep layers or lateral vs. medial divisions? Brain Res Brain Res Rev 2003, 42: 243–251.
33. Shipley MT, Ennis M. Functional organization of olfactory system. J Neurobiol 1996, 30: 123–176.
34. Ke MT, Fujimoto S, Imai T. SeeDB: a simple and morphology-preserving optical clearing agent for neuronal circuit reconstruction. Nat Neurosci 2013, 16: 1154–1161.
35. De Saint Jan D, Hirnet D, Westbrook GL, Charpak S. External tufted cells drive the output of olfactory bulb glomeruli. J Neurosci 2009, 29: 2043–2052.
36. Liu S, Plachez C, Shao Z, Puche A, Shipley MT. Olfactory bulb short axon cell release of GABA and dopamine produces a temporally biphasic inhibition-excitation response in external tufted cells. J Neurosci 2013, 33: 2916–2926.
37. Kiyokage E, Pan YZ, Shao Z, Kobayashi K, Szabo G, Yanagawa Y, *et al.* Molecular identity of periglomerular and short axon cells. J Neurosci 2010, 30: 1185–1196.
38. Gire DH, Franks KM, Zak JD, Tanaka KF, Whitesell JD, Mulligan AA, *et al.* Mitral cells in the olfactory bulb are mainly excited through a multistep signaling path. J Neurosci 2012, 32: 2964–2975.
39. Murphy GJ, Darcy DP, Isaacson JS. Intraglomerular inhibition: signaling mechanisms of an olfactory microcircuit. Nat Neurosci 2005, 8: 354–364.
40. Najac M, Sanz Diez A, Kumar A, Benito N, Charpak S, De Saint Jan D. Intraglomerular lateral inhibition promotes spike timing variability in principal neurons of the olfactory bulb. J Neurosci 2015, 35: 4319–4331.
41. Parsa PV, D'Souza RD, Vijayaraghavan S. Signaling between periglomerular cells reveals a bimodal role for GABA in modulating glomerular microcircuitry in the olfactory bulb. Proc Natl Acad Sci U S A 2015, 112: 9478–9483.
42. Liu S, Puche AC, Shipley MT. The interglomerular circuit potently inhibits olfactory bulb output neurons by both direct and indirect pathways. J Neurosci 2016, 36: 9604–9617.
43. Banerjee A, Marbach F, Anselmi F, Koh MS, Davis MB, Garcia da Silva P, *et al.* An interglomerular circuit gates glomerular output and implements gain control in the mouse olfactory bulb. Neuron 2015, 87: 193–207.
44. Burton SD, LaRocca G, Liu A, Cheetham CE, Urban NN. Olfactory bulb deep short-axon cells mediate widespread inhibition of tufted cell apical dendrites. J Neurosci 2017, 37: 1117–1138.
45. Eyre MD, Antal M, Nusser Z. Distinct deep short-axon cell subtypes of the main olfactory bulb provide novel intrabulbar and extrabulbar GABAergic connections. J Neurosci 2008, 28: 8217–8229.

46. Pressler RT, Strowbridge BW. Blanes cells mediate persistent feedforward inhibition onto granule cells in the olfactory bulb. Neuron 2006, 49: 889–904.
47. Eyre MD, Kerti K, Nusser Z. Molecular diversity of deep short-axon cells of the rat main olfactory bulb. Eur J Neurosci 2009, 29: 1397–1407.
48. Kelsch W, Sim S, Lois C. Watching synaptogenesis in the adult brain. Annu Rev Neurosci 2010, 33: 131–149.
49. Belluscio L, Lodovichi C, Feinstein P, Mombaerts P, Katz LC. Odorant receptors instruct functional circuitry in the mouse olfactory bulb. Nature 2002, 419: 296–300.
50. Lodovichi C, Belluscio L, Katz LC. Functional topography of connections linking mirror-symmetric maps in the mouse olfactory bulb. Neuron 2003, 38: 265–276.
51. Brunjes PC, Illig KR, Meyer EA. A field guide to the anterior olfactory nucleus (cortex). Brain Res Brain Res Rev 2005, 50: 305–335.
52. Yan Z, Tan J, Qin C, Lu Y, Ding C, Luo M. Precise circuitry links bilaterally symmetric olfactory maps. Neuron 2008, 58: 613–624.
53. Illig KR, Eudy JD. Contralateral projections of the rat anterior olfactory nucleus. J Comp Neurol 2009, 512: 115–123.
54. Boyd AM, Sturgill JF, Poo C, Isaacson JS. Cortical feedback control of olfactory bulb circuits. Neuron 2012, 76: 1161–1174.
55. Insausti R, Herrero MT, Witter MP. Entorhinal cortex of the rat: cytoarchitectonic subdivisions and the origin and distribution of cortical efferents. Hippocampus 1997, 7: 146–183.
56. de la Rosa-Prieto C, Ubeda-Banon I, Mohedano-Moriano A, Pro-Sistiaga P, Saiz-Sanchez D, Insausti R, *et al.* Subicular and CA1 hippocampal projections to the accessory olfactory bulb. Hippocampus 2009, 19: 124–129.
57. de Olmos J, Hardy H, Heimer L. The afferent connections of the main and the accessory olfactory bulb formations in the rat: an experimental HRP-study. J Comp Neurol 1978, 181: 213–244.
58. van Groen T, Wyss JM. Extrinsic projections from area CA1 of the rat hippocampus: olfactory, cortical, subcortical, and bilateral hippocampal formation projections. J Comp Neurol 1990, 302: 515–528.
59. Devore S, de Almeida L, Linster C. Distinct roles of bulbar muscarinic and nicotinic receptors in olfactory discrimination learning. J Neurosci 2014, 34: 11244–11260.
60. Bendahmane M, Ogg MC, Ennis M, Fletcher ML. Increased olfactory bulb acetylcholine bi-directionally modulates glomerular odor sensitivity. Sci Rep 2016, 6: 25808.
61. Hamamoto M, Kiyokage E, Sohn J, Hioki H, Harada T, Toida K. Structural basis for cholinergic regulation of neural circuits in the mouse olfactory bulb. J Comp Neurol 2017, 525: 574–591.
62. Gracia-Llanes FJ, Crespo C, Blasco-Ibanez JM, Nacher J, Varea E, Rovira-Esteban L, *et al.* GABAergic basal forebrain afferents innervate selectively GABAergic targets in the main olfactory bulb. Neuroscience 2010, 170: 913–922.
63. Nunez-Parra A, Maurer RK, Krahe K, Smith RS, Araneda RC. Disruption of centrifugal inhibition to olfactory bulb granule cells impairs olfactory discrimination. Proc Natl Acad Sci U S A 2013, 110: 14777–14782.
64. Escanilla O, Arrellanos A, Karnow A, Ennis M, Linster C. Noradrenergic modulation of behavioral odor detection and discrimination thresholds in the olfactory bulb. Eur J Neurosci 2010, 32: 458–468.
65. Escanilla O, Alperin S, Youssef M, Ennis M, Linster C. Noradrenergic but not cholinergic modulation of olfactory bulb during processing of near threshold concentration stimuli. Behav Neurosci 2012, 126: 720–728.
66. Doucette W, Milder J, Restrepo D. Adrenergic modulation of olfactory bulb circuitry affects odor discrimination. Learn Mem 2007, 14: 539–547.
67. Li G, Linster C, Cleland TA. Functional differentiation of cholinergic and noradrenergic modulation in a biophysical model of olfactory bulb granule cells. J Neurophysiol 2015, 114: 3177–3200.
68. Zhou FW, Dong HW, Ennis M. Activation of beta-noradrenergic receptors enhances rhythmic bursting in mouse olfactory bulb external tufted cells. J Neurophysiol 2016, 116: 2604–2614.
69. Gire DH, Schoppa NE. Long-term enhancement of synchronized oscillations by adrenergic receptor activation in the olfactory bulb. J Neurophysiol 2008, 99: 2021–2025.
70. Zhong W, Li Y, Feng Q, Luo M. Learning and stress shape the reward response patterns of serotonin neurons. J Neurosci 2017, 37: 8863–8875.
71. Fonseca MS, Murakami M, Mainen ZF. Activation of dorsal raphe serotonergic neurons promotes waiting but is not reinforcing. Curr Biol 2015, 25: 306–315.
72. Liu ZX, Zhou JF, Li Y, Hu F, Lu Y, Ma M, *et al.* Dorsal raphe neurons signal reward through 5-HT and glutamate. Neuron 2014, 81: 1360–1374.
73. Liu Y, Jiang Y, Si Y, Kim JY, Chen ZF, Rao Y. Molecular regulation of sexual preference revealed by genetic studies of 5-HT in the brains of male mice. Nature 2011, 472: 95–99.
74. Kraus C, Castren E, Kasper S, Lanzenberger R. Serotonin and neuroplasticity - Links between molecular, functional and structural pathophysiology in depression. Neurosci Biobehav Rev 2017, 77: 317–326.
75. Luo MM, Li Y, Zhong WX. Do dorsal raphe 5-HT neurons encode "beneficialness"? Neurobiol Learn Mem 2016, 135: 40–49.
76. Miyazaki KW, Miyazaki K, Tanaka KF, Yamanaka A, Takahashi A, Tabuchi S, *et al.* Optogenetic activation of dorsal raphe serotonin neurons enhances patience for future rewards. Curr Biol 2014, 24: 2033–2040.
77. Huang Z, Thiebaud N, Fadool DA. Differential serotonergic modulation across the main and accessory olfactory bulbs. J Physiol 2017, 595: 3515–3533.
78. Steinfeld R, Herb JT, Sprengel R, Schaefer AT, Fukunaga I. Divergent innervation of the olfactory bulb by distinct raphe nuclei. J Comp Neurol 2015, 523: 805–813.
79. Liu SL, Aungst JL, Puche AC, Shipley MT. Serotonin modulates the population activity profile of olfactory bulb external tufted cells. J Neurophysiol 2012, 107: 473–483.
80. Brill J, Shao Z, Puche AC, Wachowiak M, Shipley MT. Serotonin increases synaptic activity in olfactory bulb glomeruli. J Neurophysiol 2016, 115: 1208–1219.
81. Schmidt LJ, Strowbridge BW. Modulation of olfactory bulb network activity by serotonin: synchronous inhibition of mitral cells mediated by spatially localized GABAergic microcircuits. Learn Mem 2014, 21: 406–416.
82. Petzold GC, Hagiwara A, Murthy VN. Serotonergic modulation of odor input to the mammalian olfactory bulb. Nat Neurosci 2009, 12: 784–791.
83. Brunert D, Tsuno Y, Rothermel M, Shipley MT, Wachowiak M. Cell-type-specific modulation of sensory responses in olfactory bulb circuits by serotonergic projections from the raphe nuclei. J Neurosci 2016, 36: 6820–6835.